remote sensing

MDPI

Article

Hyperspectral Band Selection for Crop Identification and Mapping of Agriculture

Yulei Tan [1], Jingtao Gu [2], Laijun Lu [3], Liyuan Zhang [1], Jianyu Huang [1], Lin Pan [1], Yan Lv [4], Yupeng Wang [1] and Yang Chen [1,*]

[1] School of Computer Technology and Engineering, Changchun Institute of Technology, Changchun 130012, China; tanyulei@ccit.edu.cn (Y.T.); zhangly@ccit.edu.cn (L.Z.); huangjy@ccit.edu.cn (J.H.); panlin@ccit.edu.cn (L.P.); wangyupeng@stu.ccit.edu.cn (Y.W.)
[2] College Student Employment and Entrepreneurship Guidance Center, Changchun Institute of Technology, Changchun 130012, China; 0202055@ccit.edu.cn
[3] College of Earth Sciences, Jilin University, Changchun 130061, China; lulj@jlu.edu.cn
[4] College of Information Technology, Jilin Agricultural University, Changchun 130118, China; lvyan@jlau.edu.cn
* Correspondence: chenyang@ccit.edu.cn

Abstract: Different crops, as well as the same crop at different growth stages, display distinct spectral and spatial characteristics in hyperspectral images (HSIs) due to variations in their chemical composition and structural features. However, the narrow bandwidth and closely spaced spectral channels of HSIs result in significant data redundancy, posing challenges to crop identification and classification. Therefore, the dimensionality reduction in HSIs is crucial. Band selection as a widely used method for reducing dimensionality has been extensively applied in research on crop identification and mapping. In this paper, a crop superpixel-based affinity propagation (CS-AP) band selection method is proposed for crop identification and mapping in agriculture using HSIs. The approach begins by gathering crop superpixels; then, a spectral band selection criterion is developed by analyzing the variations in the spectral and spatial characteristics of crop superpixels. Finally, crop identification bands are determined through an efficient clustering approach, AP. Two typical agricultural hyperspectral data sets, the Salinas Valley data set and the Indian Pines data set, are selected for validation, each containing 16 crop classes, respectively. The experimental results show that the proposed CS-AP method achieves a mapping accuracy of 92.4% for the Salinas Valley data set and 88.6% for the Indian Pines data set. When compared to using all bands, two unsupervised band selection techniques, and three semi-supervised band selection techniques, the proposed method outperforms others with an improvement of 3.1% and 4.3% for the Salinas Valley and Indian Pines data sets, respectively. Indicate that the proposed CS-AP method achieves superior mapping accuracy by selecting fewer bands with greater crop identification capability compared to the other band selection methods. This research's significant results demonstrate the potential of this approach in precision agriculture, offering a more cost-effective and timely solution for large-scale crop mapping and monitoring in the future.

Keywords: hyperspectral imagery; crop identification; band selection; superpixels; remote sensing

check for updates

Academic Editor: Eileen H. Helmer

Received: 9 December 2024
Revised: 27 January 2025
Accepted: 13 February 2025
Published: 15 February 2025

Citation: Tan, Y.; Gu, J.; Lu, L.; Zhang, L.; Huang, J.; Pan, L.; Lv, Y.; Wang, Y.; Chen, Y. Hyperspectral Band Selection for Crop Identification and Mapping of Agriculture. *Remote Sens.* **2025**, *17*, 663. https://doi.org/10.3390/rs17040663

Copyright: © 2025 by the authors. Licensee MDPI, Basel, Switzerland. This article is an open access article distributed under the terms and conditions of the Creative Commons Attribution (CC BY) license (https://creativecommons.org/licenses/by/4.0/).

1. Introduction

Hyperspectral images (HSIs) capture data across hundreds of contiguous and narrow spectral bands from the visible to the infrared spectrum [1,2], so the crops exhibit continuous

and fine spectral reflectance characteristics in HSIs [3,4]. The spectral curve of each crop is unique due to its chemical composition (like chlorophyll, water, nitrogen content, etc.) and structural characteristics (like leaf thickness, surface roughness, etc.), which can distinguish various crops or the same crop at different growth cycles [5,6]. This continuous and fine spectral reflectance information makes HSIs particularly valuable for applications of crop mapping and agricultural analysis [7,8].

Despite their potential, HSIs pose several significant challenges for crop classification and mapping classification tasks. First, the Hughes phenomenon (or the curse of dimensionality) can arise when the classification accuracy declines with an increase in spectral bands, especially when labeled training samples are scarce [9,10]. Second, the high degree of correlation between spectral bands leads to redundant information, which can negatively impact classification effectiveness. Third, the crop chemical composition and the high spatial resolution of HSIs often reducing inter-class separability, making it harder to distinguish among various land cover classes within the spectral domain [11]. To address these challenges, it was essential to reduce the dimensionality of the data and eliminate redundant spectral information while enhancing the ability to discriminate between pixels from different classes.

Dimensionality reduction (DR) is an essential preprocessing step that reduces the number of hyperspectral channels to enhance the classification performance of HSIs [12,13]; band selection is one of the most common DR methods currently [14,15]. Depending on the availability of the existing knowledge, band selection algorithms can be categorized into unsupervised [16], supervised [17], and semi-supervised [18] approaches. Unsupervised methods [19,20] utilize statistical measures to identify informative bands by clustering features and selecting cluster centers, i.e., bands. Examples include maximum-variance principal component analysis (MVPCA) [21], k-means clustering [22], information divergence (ID) [23,24], and the Gaussian mixture model (GMM) [23]. Supervised methods [25,26] select subsets of bands by evaluating class separability using prior knowledge. Common examples include linear discriminant analysis (LDA) [27,28] and random forest (RF) [29]. Semi-supervised methods [30] are among the most widely used techniques for HSIs' classification. They typically leverage a small amount of prior information, such as crop labels, to reduce HSI dimensionality. Examples include the semi-supervised support vector machine [31] and the semi-supervised random forest [32].

For crop mapping, the band selection technology for hyperspectral approaches has been widely applied [7,33]. For instance, Sarma et al. [34] explore the use of evolutionary optimization algorithms, specifically Grey Wolf Optimization (GWO) and Ant Lion Optimization (ALO), to enhance band selection in high-resolution hyperspectral imaging from drones for agricultural applications. Agilandeeswari et al. [35] utilized entropy, the Normalized Difference Vegetation Index (NDVI), and the Modified Normalized Difference Water Index (MNDWI) to select and quantize bands within the visible, near-infrared, and shortwave infrared regions. Rabi et al. [36] introduced a hybrid method integrating radiative transfer modeling with a machine learning (ML) algorithm to estimate the leaf area index (LAI) and canopy chlorophyll content (CCC) of wheat fields. Zhang et al. [37] proposed an innovative hybrid approach that integrates amplitude- and shape-enhanced 2D correlation spectroscopy with transfer learning to estimate leaf chlorophyll content (LCC) in winter wheat from hyperspectral data. Kang et al. [38] introduced a feature clustering algorithm for hyperspectral imagery with a focus on interpretability. The approach begins with a simulated perception process and proposes an interpretable band selection algorithm to reduce data dimensionality. Cheng et al. [39] introduced a graph-based RNN framework, GT-long-short-term memory (LSTM), for band selection to predict winter wheat yield at the county scale.

Affinity propagation (AP) [40], as an exemplar-based clustering algorithm, has been extensively used for band selection in HSIs [41–43]. However, a limitation of AP is its sensitivity to initialization, which can result in an unstable subset of selected bands that may vary, depending on the initial conditions. To address this, a series of improved AP-based methods have been developed to ensure that the selected bands are more stable and exhibit relatively low redundancy. For example, Yang et al. [44,45] utilized a feature metric derived from related component analysis with chunklets and proposed the FM-AP method. Superpixel is an image segmentation technique that partitions an image into several smaller regions, where each segmented pixel block is referred to as a superpixel [46]. The simple linear iterative clustering (SLIC) algorithm [47] is a commonly used superpixel technique that relies on k-means clustering. It efficiently generates regular superpixels that adhere well to boundaries and is particularly popular in the analysis of HSIs [48,49]. For example, Tan et al. [50] proposed a lithologic-superpixel-based band selection (LSBS) that utilizes related component analysis and AP to identify a set of selected bands. Yang et al. [51] proposed an unsupervised band selection for land cover classification using superpixels. Adjacent similar pixels in HSIs are likely to belong to the same crop unit and typically exhibit a regional distribution in the spatial domain, indicating spatial correlation. Thus, HSIs can be segmented into distinct crop superpixels.

In this paper, the proposed crop superpixel-based affinity propagation (CS-AP) approach considers both the spatial and spectral variability characteristics of crop pixels for crop identification and mapping using HSIs, as is shown in Figure 1. The key contributions of this paper are as follows: (1) A novel principal component feature space, termed crop superpixels (CSs), is constructed using principal component analysis (PCA), combined with the SLIC superpixel algorithm. (2) A band selection criterion is defined based on relevant component analysis (RCA), aimed at estimating and minimizing the within-CSs covariance of the data and leveraging the strong homogeneity and uniformity within the CSs. (3) A band selection approach is introduced by incorporating the defined band selection criterion with the AP algorithm to select bands that exhibit high homogeneity within the same crop and a low spectral correlation between different bands. The effectiveness of the proposed band selection method is evaluated using two AVIRIS hyperspectral data sets: Salinas Valley, California, USA, and Indian Pines 92AV3C in northwest Indiana. The mapping performance of the proposed method is evaluated and compared with all spectral channels (as a baseline), as well as two unsupervised and three semi-supervised band selection methods.

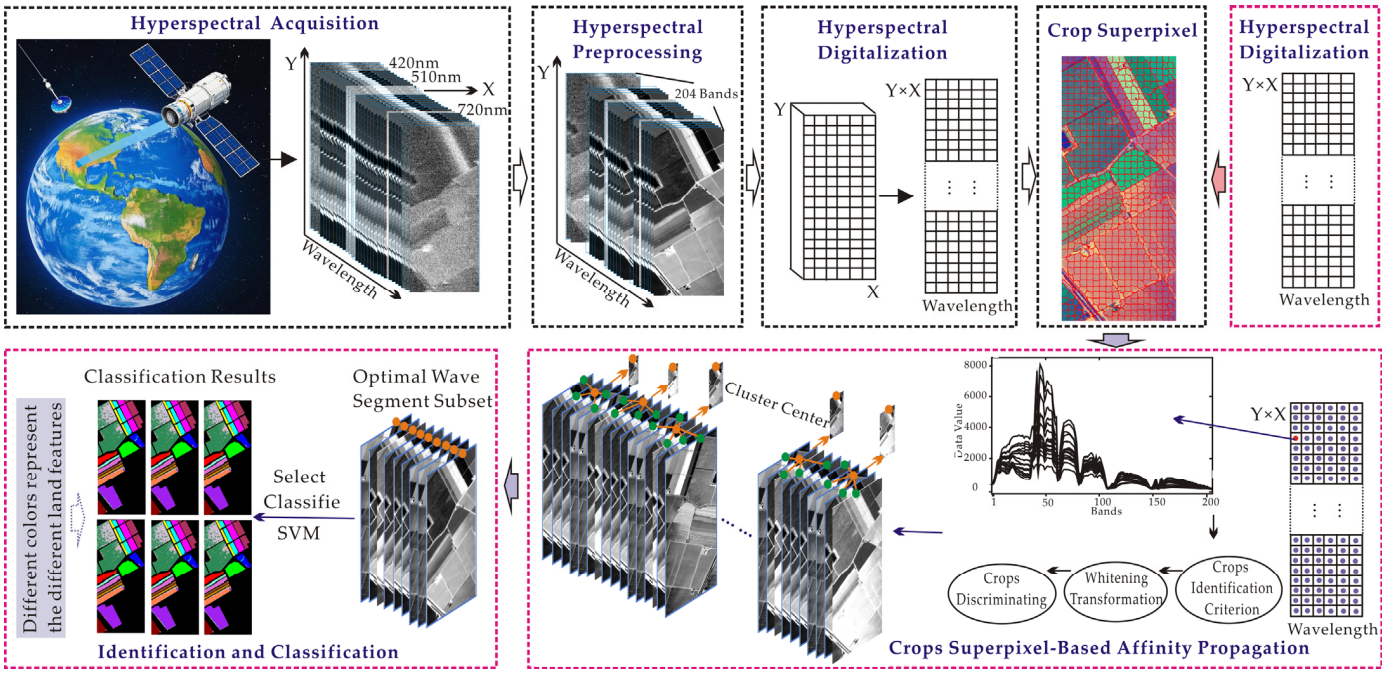


Figure 1. Crop identification and mapping flowchart.

2. Methods

In this section, the proposed CS-AP method comprises two key components: (i) crop superpixels (CSs) generation and (ii) the selection of representative band subsets based on AP clustering using the CSs. A comprehensive explanation and overview of these two parts are provided in the following subsections.

2.1. Crop Superpixels Generation

Considering the spatial regional characteristics and the spectral variability of different crops or the same crop in different growth cycles, crop superpixels (CSs) have been given to improve the performance of crop identification and discrimination. In a conventional SLIC algorithm, the similarity and proximity of pixels are determined based on color information in images [52]. Here, the PCA [53] has been introduced into SLIC superpixels, and the strong correlation spectra feature will reduce between different growth cycles of the same crops for the subtle difference between crops' spectral information. Next, adjacent pixels with spatial proximity are identified by calculating the spatial distance based on the coordinates of each pixel. In order to segment the CSs in HSIs, the distinction of crop spectra is defined based on PCA to extract the "most informative" feature.

Let $X = \{x_1, x_2, \ldots, x_N\} \in \mathbf{R}^{B \times N}$ represent the set of pixel vectors from the HSIs' pixel vectors, where $x_i = \{x_{i1}, x_{i2}, \ldots, x_{iB}\}$ $(i = 1, 2, \ldots, N)$, x_i is the i-th spectral pixel vector in the band space of the HSIs band space, N denotes the total number of pixels in the HSIs, and B indicates the number of spectral bands. Thus, the principal component covariance matrix P_{CS} in HSIs can be calculated as follows:

$$P_{CS} = \frac{1}{N-1} X'^{T} X', \tag{1}$$

where X' is the standardized HSI pixel vectors. Meanwhile, the eigenvalues and eigenvectors can be expressed as follows:

$$P_{CS} E = E\lambda, \tag{2}$$

where E is the eigenvectors for an orthogonal matrix, and $E^{-1} = E^{T}$, λ is the eigenvalues of HSIs pixel vectors. Then, the features will transform to find a linear transformation

matrix, V, which can greatly distinguish the spectral features between crop pixels. The transformation formula is as follows:

$$V = E^T \cdot P_{CS} \cdot E, \tag{3}$$

The most informative feature usually concentrates on the first three principal components of the linear transformation matrix; subsequently, these principal components are extracted as the pixel similarity and proximity features, $X_{[f,p,q]}$, of CSs, and they can be expressed as follows:

$$X_{[f,p,q]} = X \cdot V_{[f,p,q]}, \tag{4}$$

where f,p,q are the HSIs pixels' principal components feature space, the spectral and spatial similarity of crop spectrums, S_{CS}, based on the SLIC superpixels in HSIs can be calculated as follows:

$$S_{CS} = \sqrt{\frac{\Delta f^2 + \Delta p^2 + \Delta q^2}{(N_f)^2} + \frac{\Delta g^2 + \Delta h^2}{(N_c)^2} + \lambda \Delta I}, \tag{5}$$

where N_f is the respective maximum distances within d_f, representing the weight for feature similarity, N_c is the respective maximum distances within d_c, representing the spatial proximity that satisfies $N_c = (N/K)^{1/2}$, K is the number of crop superpixels, and g_i and h_j are the pixel's coordinate position. ΔI is the gradient at a pixel location.

Figure 2 illustrates the flowchart for generating crop superpixels. Four pixel points marked in the HSIs' principal components feature space with blue, celeste, and purple represent three distinct crop units, i.e., Lettuce_5wk, Lettuce_6wk, and Brocoli_weeds_2. As one can see from the HIS distance space, the spatial distance between the blue and celeste pixels is almost equal to the spatial distance between the two purple pixels, which is determined according to the actual geographical location of the pixels. From the single band image of HSI, the color feature differences between the blue and celeste pixels are relatively slight due to the fact that the two pixels are related to different growth cycles of lettuce. However, from the principal component feature, there are significant feature differences between the blue and celeste pixels that have been segmented into different crop superpixels, which indicates that principal component feature analysis has strong recognition capabilities for different growth cycles of the same crop. Here, it is worth noting that the two purple pixels have the same features in both the single band image and the principal component feature space of HIS, and they can also be segmented into different crop superpixel units due to their spatial distance, indicating that adjacent crop superpixel units may belong to the same crop or different crops, but the interior of the crop superpixel unit is assumed to belong to the same crop.

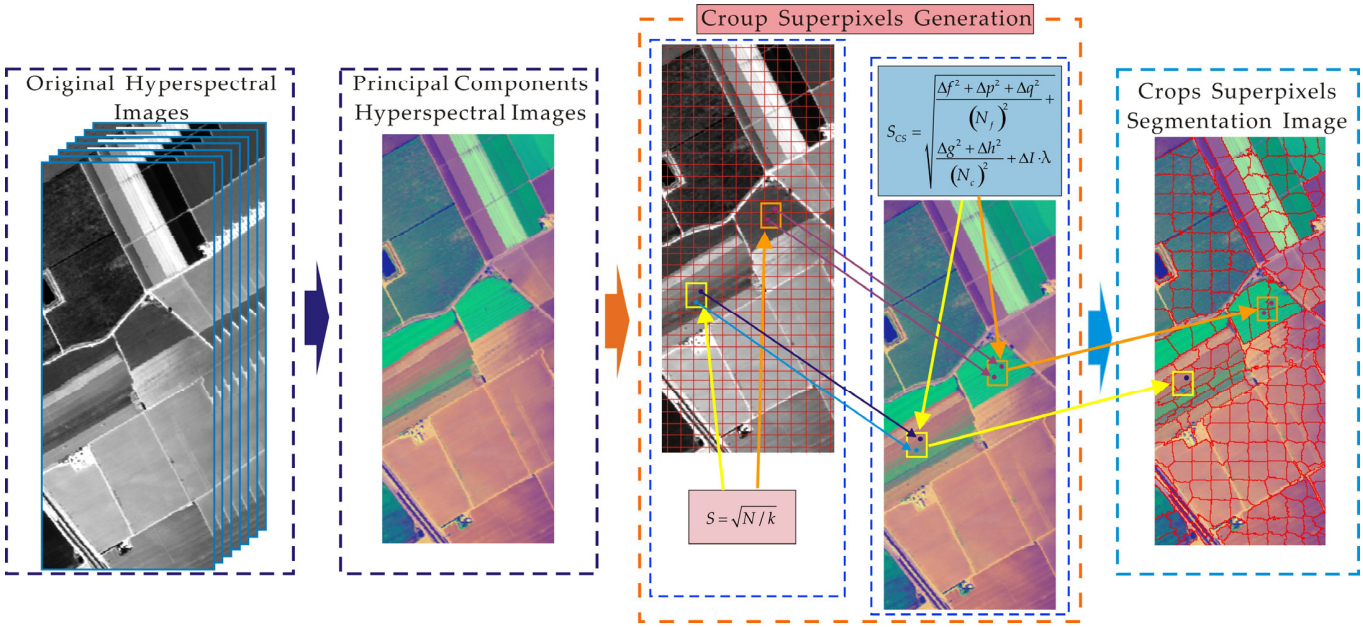


Figure 2. Flowchart of the crop superpixel (CS) generation process.

2.2. Crop Superpixel-Based AP

The target of the band section is to locate $Y = \{y_1, y_2, \ldots, y_f\}$ (f << B) optimal crops' identification bands' subset from $X^T = \{x_1, x_2, \ldots, x_B\}$ within HSI spectral channels. The crop superpixel learned here is based on the RCA [54,55]; the selected optimal bands should offer high a crop feature identification capability for different crop types or different growth cycles of the same crops. The pixels within the same crop superpixels must have high relevance. Meanwhile, low redundancy is an important indicator for the optimal bands subset. Accordingly, the within-CSs covariance matrix based on crop superpixels can be defined as follows:

$$\hat{C}_{CS} = \frac{1}{NCS} \sum_{k=1}^{NCS} \sum_{l=1}^{n_k} (x_{kl} - \overline{m}_k)(x_{kl} - \overline{m}_k)^T, \tag{6}$$

where NCS indicates the total numbers of CSs, n_k refers to the total pixel count in the k-th CSs, x_{kl} represents the l-th pixel in the k-th CSs, and m_k denotes the mean of the k-th CSs, which should be written as follows:

$$\overline{m}_k = \frac{1}{n_k} \sum_{l=1}^{n_k} x_{kl}, \tag{7}$$

The adopted band selection criterion is the key to band selection performance. Here, a crop identification band selection (CIBS) criterion is learned based on the RCA, which learns a whitening transformation to minimize within-CSs covariance. According to the Fisher theory [56] and derived methods [57], the within-CSs covariance matrix, i.e., the whitening transformation matrix can be written as follows:

$$W_{CS} = \frac{1}{\sqrt{\hat{C}_{CS}}}, \tag{8}$$

Following the above, the most informative feature of CSs should use the *CIBS* for measurements. The *CIBS* among different bands, x_i and x_j, can be expressed as follows:

$$CIBS(x_i, x_j) = W_{CS}(x_i, x_j), \tag{9}$$

where $i = 1, 2, \ldots, B$, $j = 1, 2, \ldots, B$, $W_{CS}(x_i, x_j)$ is the (x_i, x_j) element with W_{CS}. $CIBS(x_i, x_j)$ is employed to assess the most informative feature between two different bands.

The crop-discriminating capability of a single band, x_i, can be calculated as follows:

$$CIBS(x_i, x_j) = \frac{-CTS_{CS}}{W_{CS}(x_i, x_j)}, \tag{10}$$

where $i = 1, 2, \ldots, B$; CTS_{CS} is the crop threshold scalar for CSs, which is usually used to set an appropriate value to achieve the desired number of selected bands. The defined *CIBS* is then utilized as an input to the AP algorithm [40]. In the AP, a common choice for feature measurement is the negative Euclidean distance (ED). However, in the proposed CS-AP method, self-similarity $CIBS(x_i, x_i)$ is utilized to measure the crop identification capability of each band.

In AP clustering, the goal is to determine the optimal set of cluster centers (or exemplars) that maximize the total similarity between each point and its respective center. AP is based on a factor graph constructed from overall similarity values, where the responsibility and availability of two messages are exchanged between data points. Responsibility reflects how suitable a candidate exemplar is as a cluster center, while availability measures how appropriate it is for a data point to belong to the cluster of a specific candidate exemplar. As AP iterates, these messages are propagated through the factor graph, accounting for different forms of competition. Once the AP algorithm converges, the cluster centers are identified through the computation of availability and responsibility messages for each data point.

Initially, the availability values $a(x_i, x_j)$ are initialized to zero. The responsibility and availability between two bands are updated using a max-product algorithm as follows:

$$r(x_i, x_j) = CIBS(x_i, x_j) - \max_{q \neq j} \{CIBS(x_i, x_q) + a(x_i, x_q)\}, \tag{11}$$

$$a(x_i, x_j) = \begin{cases} \min\left\{0, r(x_i, x_j) + \sum\limits_{p \neq i,j} \max\{0, r(x_p, x_j)\}\right\} & i \neq j \\ \sum\limits_{p \neq j} \max\{0, r(x_p, x_j)\} & i = j \end{cases}, \tag{12}$$

where the responsibility $r(x_i, x_j)$ quantifies how strongly band x_j is suited to act as the exemplar (or cluster center) for band x_i, the availability $a(x_i, x_j)$ represents the degree to which x_j can appropriately serve as the representative for x_i. Here, x_q and x_p refer to the q-th and p-th bands, respectively. The responsibility update enables all candidate exemplars to compete for the assignment of a band. During responsibility updates, potential exemplars compete to claim bands as members, while the availability update checks the validity of each candidate as a cluster center.

In the first iteration, this competition is solely driven by data; however, in later iterations, once specific bands are allocated to exemplars, the availability values may drop below zero as described by Equation (12). Negative availability values effectively lower some $CIBS(x_i, x_j)$ values, thus eliminating specific candidate exemplars from further consideration. The self-responsibility $r(x_i, x_j)$ aggregates evidence suggesting that band x_j is a valid exemplar. The positive parts of incoming responsibilities contribute to the update when $i \neq j$,. A negative self-responsibility value, $r(x_i, x_j)$, implies that band x_j does not qualify as an exemplar. However, if certain bands have positive responsibility values toward x_j, this can raise the value of x_j to availability as an exemplar, up to a limit of zero, to prevent excessive influence from strongly positive responsibilities. The self-availability $a(x_i, x_j)$ accumulates supportive evidence from other bands' positive responsibility values directed toward candidate exemplar x_j when $i = j$, indicating that x_j may be a valid cluster center.

For any band, the highest likelihood that band x_j will serve as the final cluster center for band x_i is determined by finding the maximum combined sum availability, $a(x_i, x_j)$, and responsibility, $r(x_i, x_j)$. This optimal sum indicates the strongest potential for x_j to be selected as the cluster center for x_i, following the rule outlined below.

$$\max_{x_j \in Y} \{a(x_i, x_j) + r(x_i, x_j)\}, \tag{13}$$

To avoid oscillations in the search algorithm during the calculation of responsibilities and availabilities, a damping factor is introduced. This damping process adjusts the two types of messages using the equations provided below:

$$\begin{aligned} \hat{R}^{t+1} &= \beta \hat{R}^{t-1} + (1-\beta)\hat{R}^{t} \\ \hat{A}^{t+1} &= \beta \hat{A}^{t-1} + (1-\beta)\hat{A}^{t\prime} \end{aligned} \tag{14}$$

Here, the responsibility $r(x_i, x_j)$ and availability $r(x_i, x_j)$ vectors are represented by r and a, respectively, with β as the damping factor, constrained to $0.5 \leq \beta < 1$. The parameter t denotes the iteration count, higher values of β result in slower convergence of the algorithm. The identified cluster exemplars within the set C represent the bands with strong crop feature identification capabilities. Consequently, the subset of bands Y, distinguished by high crop feature identification and minimal redundancy, can be chosen and kept.

At convergence, the final cluster representative is obtained, which includes an optimal set of bands and their corresponding quantities. These outcomes can then be utilized for crops' identification and classification.

3. Experimental Results

3.1. Regional and Data Sets' Description

Two typical agricultural hyperspectral data sets, Salinas Valley and Indian Pines (name as Indian Pines 92AV3C), were used in the experiments, and they contain various types of crops [35]. These data sets are freely available and were downloaded from [58]. The description of the two regions and their respective data sets are as follows.

The first data set [59], Salinas Valley, was collected via the Airborne Visible/Infrared Imaging Spectrometer (AVIRIS) sensor in Salinas Valley, Monterey County, California, USA. The Salinas Valley is an important agricultural area, often referred to as the "Salad Bowl of the World". Situated just 12 miles from the Pacific Ocean in central California, it is close to San Jose. The region is known for its fertile soil, mild climate, abundant sunshine, and rich agricultural production, growing over 150 different crops. The Salinas Valley is one of the largest centers of organic agriculture in the USA, and it is famous for producing artichokes, lettuce, cauliflower, and broccoli. Additionally, the valley is home to the Pinnacles National Monument, two of California's oldest missions, and several renowned vineyards, making it a leader in sustainability and agricultural technology. The Salinas Valley data set has 512 × 217 pixels with 224 spectral bands ranging from 380 to 2500 nm and 20 signal-to-noise (SNR) bands (bands 108–112, 154–167, and 224); after eliminating them, 204 bands were considered. The spatial resolution (3.7 m/pixel) was significantly improved compared with Indian Pines 92AV3C (the second data set). The data set also includes 16 crop classes that represent various crop varieties or the same crop type with different growth stages. Agricultural crops such as vineyard fields, broccoli, celery, fallow land, and lettuce cover 100% of the area [60–62]. There are a total of 54,153 true ground-labeled pixels, and 10,247 pixels (30%) are used as the training set; the pixel distribution of 16 crop classes with a description is shown in Table 1 [63]. Figure 3 displays the geographic location and data

overview of the Indian Pines 92AV3C data set, including the original image, the false-color composite image using Bands 58, 28, and 18, and the associated ground truth map.

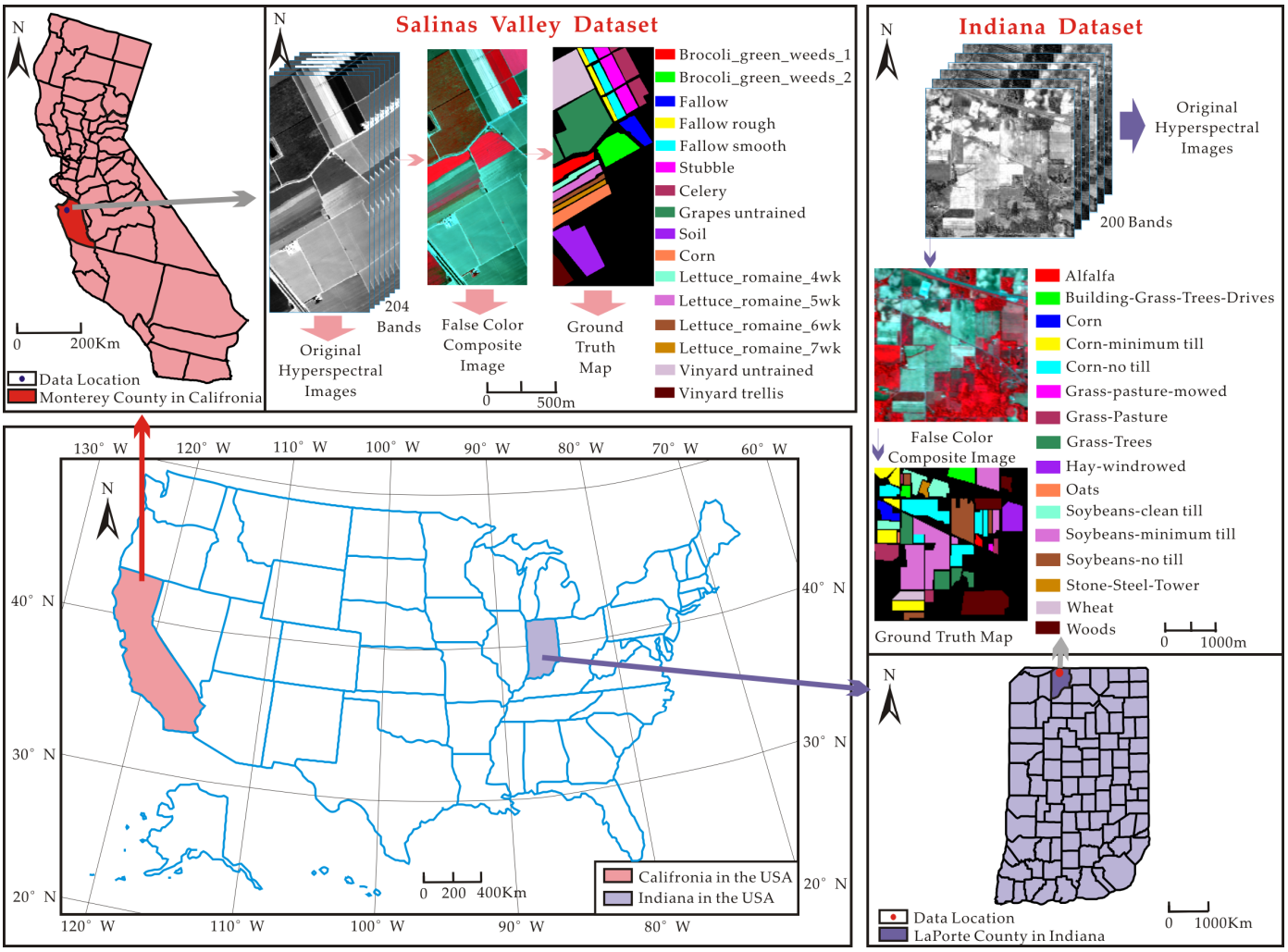


Figure 3. Geographic location and data overview of the Salinas Valley and Indian Pines 92AV3C data sets.

Table 1. The sample pixel numbers of land cover categories for the Salinas Valley data set.

Order	Class Categories	Class Description	Number of Crop Pixels	
			Training Set	Testing Set
1	Brocoli_weeds_1	Green-colored vegetable	603	1406
2	Brocoli_weeds_2	Green-colored vegetable	1118	2608
3	Fallow	Land region	582	1358
4	Fallow rough	Land region	437	1019
5	Fallow smooth	Land region	797	1859
6	Stubble	Land region	1194	2786
7	Celery	Green-colored plant region	1070	2496
8	Grapes untrained	Type of vineyard	3375	7876
9	Soil	Soil region	1872	4368
10	Corn	Green-colored plant	982	2290

Table 1. *Cont.*

Order	Class Categories	Class Description	Number of Crop Pixels	
			Training Set	Testing Set
11	Lettuce_4wk	Lettuce crops that mature in the fourth week	325	759
12	Lettuce_5wk	Lettuce crops that mature in the fifth week	572	1334
13	Lettuce_6wk	Lettuce crops that mature in the sixth week	278	648
14	Lettuce_7wk	Lettuce crops that mature in the seventh week	317	741
15	Vinyard untrained	Type of vineyard	2194	5118
16	Vinyard trellis	Type of vineyard	531	1240
	Total		16,247	37,906

The second data set [64], Indian Pines (Indian Pines 92AV3C), was the same as the first data set acquired via the AVIRIS on 12 June 1992 over northwest Indiana of LaPorte County. It has become one of the most widely used benchmark data sets in the field of hyperspectral remote sensing. Indiana is a region characterized by rich agricultural land, with major crops such as corn, soybeans, and wheat. The county's flat terrain and temperate continental climate make it suitable for large-scale crop cultivation. Indiana, as a key agricultural state in the USA, is involved not only in crop cultivation but also in livestock farming and other related industries. Hyperspectral remote sensing technology plays a significant role in monitoring crop growth, soil characteristics, and other vital information in this region. The Indian Pines data set is composed of 145 × 145 pixels with 220 spectral bands, covering wavelengths from 400 to 2500 nm and featuring a spatial resolution of 20 m. After bands with lower signal-to-noise ratios (bands 104–108, 150–163, and 220) were removed, 200 bands were chosen for analysis. The data set contains 13 crop categories and three man-made structures; with a total of 10,411 pixels labeled according to ground truth, the crop categories represent various crop types and vegetation, and the three man-made structures are closely related to agricultural production activities. Agricultural crops such as corn and soybeans cover 64% of the area, while the grass and pasture vegetation type accounts for 25% of the area [65–67]. Figure 3 displays the geographic location and data overview of the Indian Pines 92AV3C data set, including the original image, a false-color composite image using Bands 58, 28, and 18, and the associated ground truth map. The sample pixel numbers for 16 land cover categories and its description are shown in Table 2 [68]; 30% of the training set was selected, which was uniformly distributed in pixel space.

Table 2. The sample pixel numbers of land cover categories for the Indian Pines 92AV3C data set.

Order	Class Categories	Class Description	Number of Pixels	
			Training Set	Testing Set
1	Alfalfa	Type of green grass	17	39
2	Building–grass–trees–drives	Building area	114	267
3	Corn	Corn crop	70	164
4	Corn—minimum till	Corn crop cultivation with minimum tillage	254	591
5	Corn—no till	Corn crop cultivation without tillage	434	1013
6	Grass—pasture—mowed	Type of green grass	8	18
7	Grass—pasture	Type of green grass	144	335
8	Grass—trees	Type of green grass	225	524
9	Hay-windrowed	Row of cut small grain grass	147	342
10	Oats	Plant in brown color	6	14
11	Soybeans—clean till	Soya plant	185	431
12	Soybeans—minimum till	Soya crop cultivation with minimum tillage	741	1728
13	Soybeans—no till	Soya crop cultivation without tillage	293	682
14	Stone–steel–tower	Tower area	32	74
15	Wheat	Brown-colored wheat plant	64	149
16	Woods	Type of tree	392	914
	Total		3126	7285

3.2. Experimental Design

To assess the performance of the proposed CS-AP, the experimental comparison includes all the bands, as well as the two unsupervised band selection and three semi-supervised band selection methods. The detailed information of these five methods is as follows:

Baseline.

- All of the original bands, i.e., utilizing all frequency bands, 204 bands of the Salinas Valley data set and 200 bands of the Indian Pines 92AV3C data set, for crop classification and identification research.

The two unsupervised band selection methods.

- MVPCA [21]: Maximum variance-based PCA using maximum variance (MV) criteria to prioritize bands. This method focuses on selecting the most informative bands from HSI data to improve classification accuracy and reduce data volume. It combines two approaches: PCA-based criteria and classification-based criteria. The PCA-based criteria use eigen-decomposition to prioritize bands based on their variance or signal-to-noise ratio. The classification-based criteria, including minimum misclassification canonical analysis and subspace projection, aim to identify bands that maximize class separability. Compared with the PCA method in the paper.

- ED-AP [40]: Standard AP with Euclidean distance (ED). AP is a clustering algorithm that identifies a set of representative examples, or exemplars, from data points. Unlike traditional clustering methods that require the number of clusters to be predefined, AP automatically determines the optimal number of clusters by exchanging similarity messages between data points. Each data point is iteratively updated to either serve as an exemplar or be associated with the closest exemplar. Compared with the AP method in the paper.

The three semi-supervised band selection methods.

- FM-AP [44,45]: Features metric-based AP, i.e., related component analysis (RCA-based AP). It constructs a feature metric that combines two measures: the band correlation metric, which assesses the correlation between spectral bands, and the band separability metric, which evaluates how well each band discriminates between classes. Using these metrics, AP is applied to group bands based on their spectral features. Compared with the RCA and AP methods in the paper.
- LSBS [50]: SLIC superpixel with negative spectral angle mapper and AP that generates different superpixel chunklets to obtain randomly selected band numbers. This method focuses on improving lithologic discrimination in HSIs by selecting the most effective spectral bands. Through measures of the homogeneity and variation of these superpixels, it defines a criterion for selecting discriminative bands. Using AP, bands that best differentiate the lithological classes are selected. Compared with the SLIC and AP methods in the paper.
- SS-AP: The SLIC superpixel based on AP. This method uses the standard SLIC method to generate superpixels and then selects a subset of bands using AP, which is in sharp contrast to the introduction of PCA into the SLIC methods in the paper.

3.3. Results

In the experiment, the performance of the proposed CS-AP method was evaluated through a series of comparative studies using ENVI 5.3. First, how the overall accuracy (OA) achieved via CS-AP varied with the number of crop superpixels was examined. Second, the effectiveness relative to a baseline approach and five other benchmark band selection methods with the selected bands was assessed. Third, a comprehensive identification analysis of the producer's accuracy (PA) and user's accuracy (UA) for each crop category, accompanied by a detailed mapping result chart, was conducted. Finally, a parameter sensitivity analysis was performed to investigate the robustness of CS-AP. It is worth noting that, in some previous research [41,50], the support vector machine (SVM) classifier consistently delivered superior performance in HSIs' classification, especially when dealing with complex agricultural data sets. Given the focus of this manuscript on HSI analysis, the SVM classifier was chosen to validate the proposed method's effectiveness.

3.3.1. Comparison of Accuracy Compared to Crop Superpixels

Using SLIC superpixels enhanced with PCA, the Salinas Valley data set and the Indian Pines 92AV3C data set were segmented into various crop superpixels (CSs) by adjusting the segmentation threshold, *k; k* is hyper-parameter. The selection of hyper-parameter *k* underwent preliminary experimental testing, which showed that the selection of hyper-parameter *k* is closely related to the size of the image. When the image is small with a larger hyper-parameter *k*, superpixel segmentation results cannot be obtained. When the image is large with a smaller hyper-parameter *k*, different objects on the image are clearly classified into the same category. Therefore, through a manual comparative analysis, in the experiments, five different values for *k* were selected to generate varying numbers of CSs (NCS). For the Salinas Valley image, the hyper-parameters *k* corresponded to {100, 300, 500,

700, and 900}, for the NCSs, they were {119, 285, 502, 643, and 708}, and for the Indian Pines 92AV3C image, k was set to {50, 100, 150, 200, and 300} due to its small size, and obtained the NCSs were {53, 83,99, 113, and 121} for hyper-parameters k These CSs served as the input for the proposed CS-AP learning framework.

The crop mapping accuracy (measured as overall accuracy with SVM) was obtained using the proposed CS-AP method with varying numbers of CSs. For comparison, results using all spectral channels (baseline) on the two data sets are also presented. The number of selected spectral bands ranged from 5 to 60, controlled by the CTS_{CS} parameter (see Figure 4).

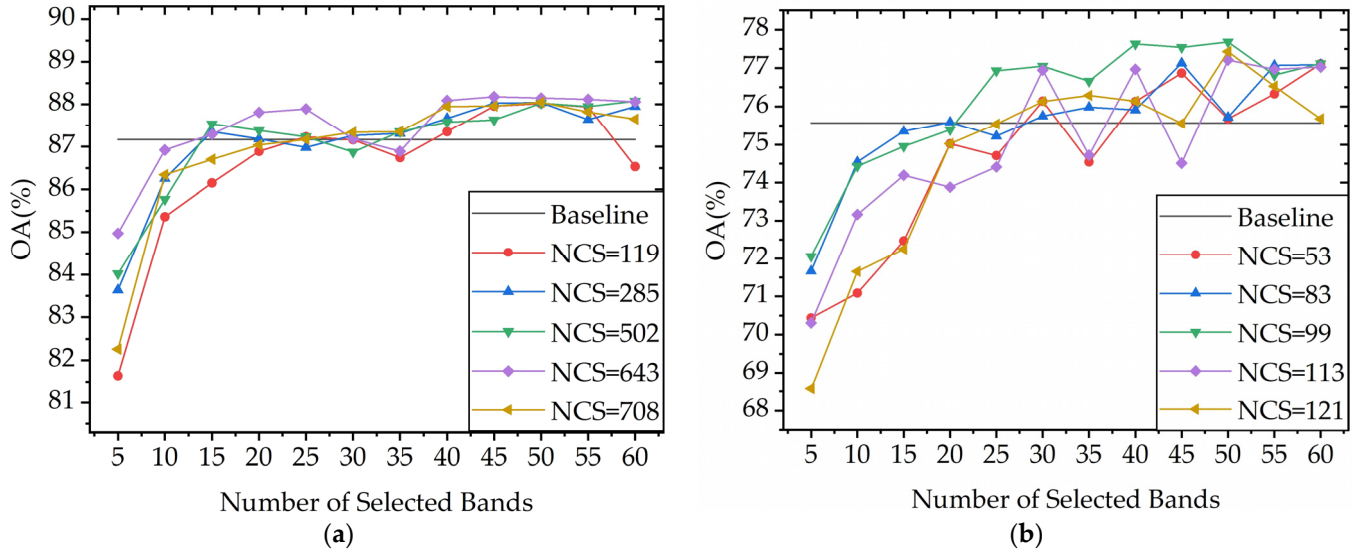


Figure 4. The overall accuracy (OA) achieved with the SVM is compared against the proposed CS-AP method with varying numbers of NCSs on (**a**) the Salinas Valley data set and (**b**) the Indian Pines 92AV3C data set. The results obtained with the baseline are also provided for comparison.

3.3.2. Accuracy Compared for the Selected Bands

The OA using the baseline and the other band selection methods mentioned in Section 3.2 were compared. Importantly, identical threshold values were applied to both the SSAP and the proposed CS-AP methods for consistency. Specifically, for the Salinas Valley data set, we set k = 700, corresponding to CS value (NCS) of 586. For the Indian Pines 92AV3C data set, k was set to 150, with CS values of 105, respectively (see Figure 5). For the Salinas Valley data set, the proposed CS-AP method demonstrated superior accuracy (Figure 5)), achieving an OA of 88.13% when 45 bands were selected; these values are superior to the 87.17% achieved with the baseline. Notably, while the SS-AP and LSBS methods achieved comparable or slightly better results than the CS-AP method when fewer bands were selected, particularly when 30 or 35 bands were selected, and the proposed CS-AP showed a dip in performance. The proposed CS-AP method delivered the highest OA when 45 bands were selected. Furthermore, with the increase in the number of selected bands, neither SS-AP nor LSBS surpassed the performance of the proposed CS-AP method. In contrast, the MVPCA and ED-AP methods consistently underperformed relative to the baseline, especially when fewer than 20 bands were selected. Even as the number of bands increased, these methods failed to achieve OA values higher than the baseline.

For the Indian Pines 92AV3C data set, the CS-AP method again outperformed the baseline, achieving an OA of 77.68%, compared to 75.57% when 25 bands were selected (Figure 5b). Although the SS-AP method also delivered competitive results, its OA was slightly lower than or on par with the proposed CS-AP method. Meanwhile, the MVPCA and ED-AP methods consistently lagged behind the baseline across all band selections. The

FM-AP and LSBS methods, on the other hand, produced an OA below the baseline when fewer than 25 bands were selected but matched or exceeded the baseline when more than 35 bands were chosen.

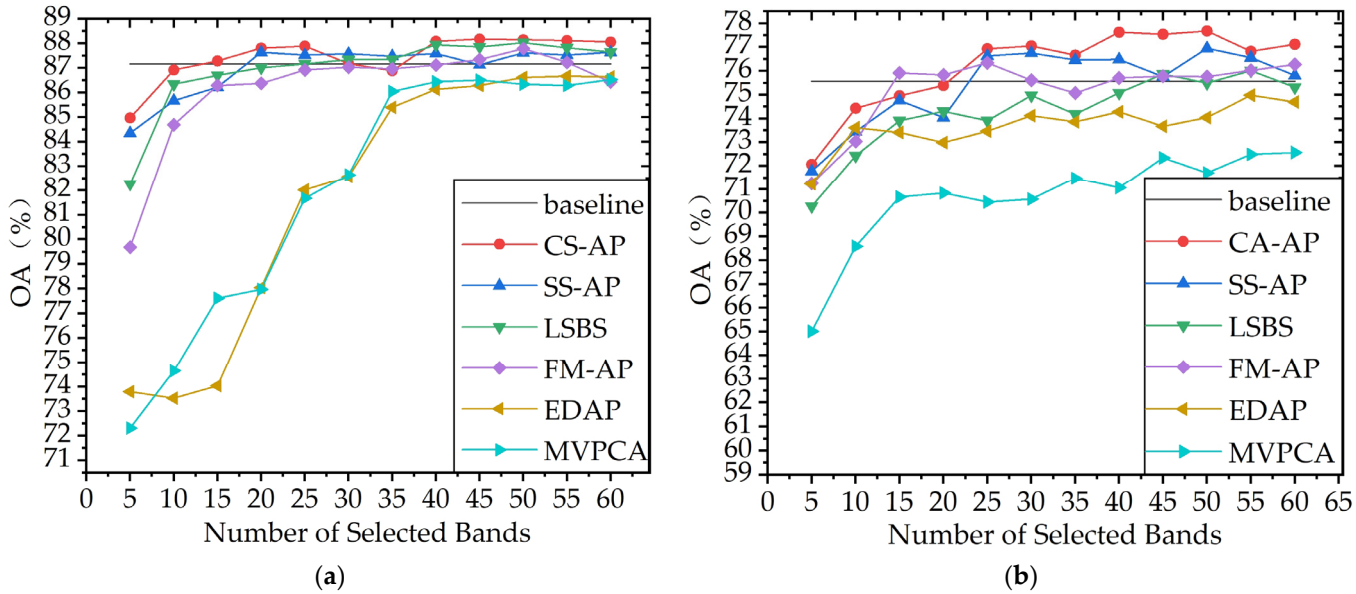


Figure 5. The overall accuracy (OA) achieved with the SVM is compared against the MVPCA, the ED-AP, the FM-AP, the LSBS, the SS-AP, the SS-AP, and the proposed CS-AP method on (**a**) the Salinas Valley data set and (**b**) the Indian Pines 92AV3C data set. The results obtained with the baseline are also provided for comparison.

Figure 6 illustrates the distribution of 45 selected bands from the Salinas Valley data set (Figure 6a) and 50 selected bands from the Indian Pines 92AV3C data set (Figure 6b) obtained using the proposed CS-AP method (NCS = 643 for Salinas Valley and NCS = 99 for Indian Pines), along with the channels selected via the MVPCA, ED-AP, FM-AP, LSBS, and SS-AP methods. For the Salinas Valley data set, one can see from Figure 6a that the adjacent spectral channels selected via the MVPCA and ED-AP methods encompass fewer distinct absorption features, limiting their effectiveness in identifying a diverse range of crop types. Specifically, the bands chosen via the ED-AP method are primarily clustered between bands 30 and 80, with additional selections between bands 80 and 150. Similarly, the MVPCA method focuses heavily on bands 60 to 100, excluding crucial absorption features for certain crops while including redundant information. In contrast, the proposed CS-AP, the SS-AP, the LSBS, and the FM-AP method exhibit a more distributed selection across the entire spectral range, capturing a broader array of relevant features. The LSBS method selects bands with an almost uniform distribution across the spectral range but neglects key discriminative bands in regions of strong absorption, such as between bands 50 and 80. A similar limitation is observed with the FM-AP method, which omits bands between 60 and 80. The proposed CS-AP method shows a more targeted approach. CS-AP predominantly selects bands around 50, 80, and 150, effectively incorporating both strong and moderate absorption features. Meanwhile, SS-AP focuses on bands around 5, 110, 145, and 200; not all of them are absorption bands. These distinctions highlight the superiority of CS-AP in capturing the essential spectral information necessary for effective crop type identification.

With the Indian Pines 92AV3C data set, one can see from Figure 6b, the MVPCA, the ED-AP, and the FM-AP method all show a relatively concentrated band distribution, especially the MVPCA method; a total of 37 bands are concentrated between bands 150 and 200, and the others are sporadically distributed from band 55 to band 130. The ED-AP method mainly concentrated on the range of bands 5 to 80 and bands 105 to 145. The distribution

of the FM-AP method is relatively scattered but concentrated in the vicinity of the 1st band, 70th band, 100th band, 140th band, and 200th band with no representative band selected between band 120 and band 190. In contrast, the proposed CS-AP, the SS-AP, and the LSBS method exhibit a more distributed selection across the entire spectral range. The LSBS method selects bands with an almost uniform distribution across the spectral range, which have a clear clustering between band 120 and band 130 but only 10 bands were selected from band 130 to 200. The proposed CS-AP method shows a more targeted approach and is relatively dense in the first 80 bands; the selected frequency band covers both strong and moderate absorption features overall. Few bands were selected within the first 80 bands for the SS-AP method relatively; we can see fewer band clusters near the 60th and 100th bands. These differences underscore the advantages of the CS-AP method in capturing the critical spectral information needed for accurate crop type identification.

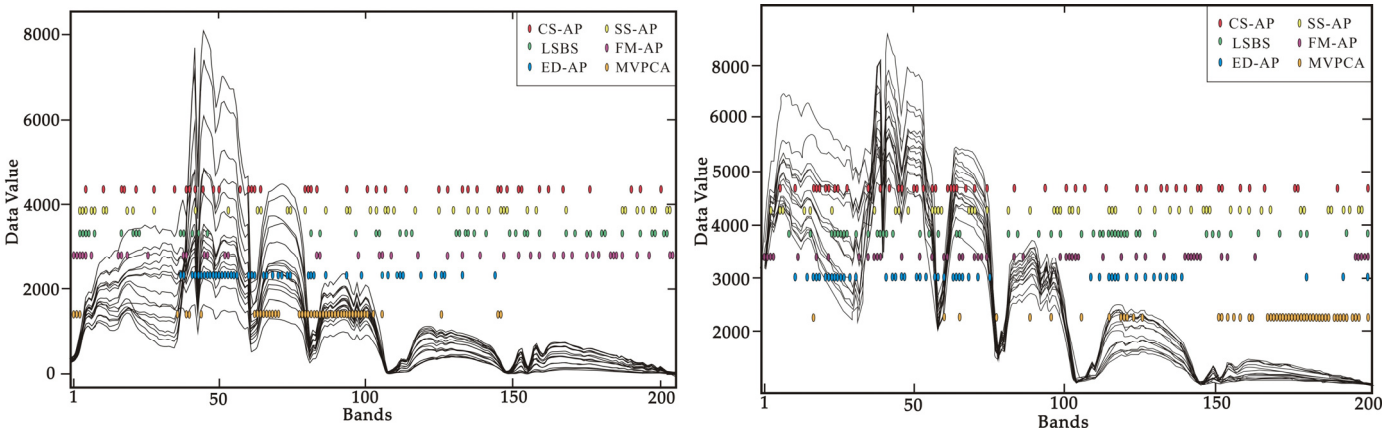


Figure 6. Data values for crop units (curves) plotted against wavelength, emphasizing the specific absorption channels and the chosen bands (indicated by elliptical points) with the proposed CS-AP, the SS-AP, the LSBS, the FM-AP, the ED-AP, and the MVPCA on (**a**) the Salinas Valley data set and (**b**) the Indian Pines 92AV3C data set.

3.3.3. Comparison of Producer's Accuracy and User's Accuracy for Crops

This experiment compared the mapping performance of all crops through the producer's accuracy (PA) and the user's accuracy (UA), along with the best OA using the baseline, the MVPCA, the ED-AP, the FM-AP, the LSBS, the SS-AP, and the proposed CS-AP method. Meanwhile, the corresponding OA and selected bands are provided.

Table 3 presents the classification accuracies achieved for the Salinas Valley data set, varying numbers of selected bands (NB). Figure 7 shows the crop identification and mapping images. The results reveal that the proposed CS-AP method consistently delivered the highest classification accuracies when 45 bands were selected, outperforming the MVPCA and ED-AP methods. Specifically, the CS-AP method achieved OA that was +1.60% and +1.43% higher than that of the MVPCA and the ED-AP method, respectively. A similar trend was observed when classification with all 204 bands. While the OA obtained via other band selection methods, such as FM-AP, LSBS, and the superpixel-based AP method (SS-AP), were comparable to those of the proposed CS-AP method, none surpassed it. Notably, the number of selected bands yielding the highest accuracies varied across methods: 60 for MVPCA, 55 for ED-AP, 50 for FM-AP and SS-AP, and 45 for LSBS. Interestingly, the CS-AP method achieved its highest accuracy with 45 bands, matching the number of bands used for LSBS.

Table 3. The PA, UA, and OA metrics achieved for the baseline, the MVPAC, the ED-AP, the FM-AP, the LSBS, the SS-AP (NCS = 586 with k = 700), and the proposed CS-AP (NCS = 643) methods were evaluated for different numbers of selected bands on the Salinas Valley data set.

Class and Accuracy		NB	Baseline	NB	MVPCA	NB	ED-AP	NB	FM-AP	NB	LSBS	NB	SS-AP	NB	CS-AP
Brocoli_green_weeds_1	PA (%)		95.02		**96.94**		96.16		96.16		96.44		96.80		96.23
	UA (%)		99.70		**100.00**		**100.00**		**100.00**		**100.00**		99.85		**100.00**
Brocoli_green_weeds_2	PA (%)		99.58		99.77		99.69		99.85		**99.89**		99.92		**99.89**
	UA (%)		97.23		97.97		97.64		97.82		97.97		**98.08**		97.86
Fallow	PA (%)		91.98		86.75		84.62		**96.76**		96.10		94.26		**96.76**
	UA (%)		92.46		91.25		89.98		95.57		95.33		95.45		**96.20**
Fallow rough	PA (%)		98.23		98.53		**98.54**		98.14		97.94		97.74		97.74
	UA (%)		94.97		95.17		95.26		**95.97**		95.69		95.31		95.59
Fallow smooth	PA (%)		94.51		93.87		93.81		96.18		96.61		96.50		**96.66**
	UA (%)		93.96		90.93		90.46		95.92		96.40		**96.66**		96.41
Stubble	PA (%)		98.64		97.99		98.06		98.71		99.03		**99.35**		99.10
	UA (%)		**100.00**		99.64		99.67		**100.00**		**100.00**		**100.00**		**100.00**
Celery	PA (%)		98.68		98.56		98.60		**98.76**		98.52		98.60		98.56
	UA (%)	204	99.31	60	99.72	55	**99.76**	50	99.15	45	99.23	50	99.68	45	99.23
Grapes untrained	PA (%)		88.51		89.00		**89.07**		88.07		88.37		84.92		88.33
	UA (%)		72.95		71.90		72.30		73.17		73.25		**73.86**		73.46
Soil	PA (%)		95.44		92.65		93.29		96.73		97.96		**98.47**		97.99
	UA (%)		98.28		98.95		**98.96**		97.37		98.48		98.26		98.03
Corn	PA (%)		75.72		76.21		75.91		76.29		76.38		75.46		**76.55**
	UA (%)		79.50		79.35		78.50		80.90		80.86		79.96		**81.27**
Lettuce_romaine_4wk	PA (%)		80.24		79.31		79.45		80.90		81.82		80.76		**82.08**
	UA (%)		78.28		65.94		67.98		84.34		93.10		**93.59**		93.26
Lettuce_romaine_5wk	PA (%)		99.85		99.85		99.70		99.85		99.85		99.63		**99.87**
	UA (%)		94.60		92.31		92.94		**96.10**		95.42		94.19		95.48
Lettuce_romaine_6wk	PA (%)		92.59		93.06		93.36		93.52		94.44		**95.68**		94.75
	UA (%)		**97.09**		96.02		95.73		96.96		96.84		96.57		96.39
Lettuce_romaine_7wk	PA (%)		93.26		94.34		**94.61**		92.99		92.18		90.30		91.91
	UA (%)		88.95		88.95		89.54		90.08		90.60		90.30		**90.69**
Vinyard untrained	PA (%)		50.61		47.91		48.87		51.78		51.88		**54.45**		52.23
	UA (%)		71.88		73.15		**74.15**		72.07		72.13		67.48		72.38
Vinyard trellis	PA (%)		96.37		95.40		95.56		97.26		97.34		**97.98**		97.58
	UA (%)		97.23		98.91		**99.16**		97.02		97.42		98.38		97.35
OA (%)			87.17		86.53		86.70		87.79		88.05		87.63		**88.13**

The bold entries in Table 3 represent the highest values of the producer's accuracy (PA) and the user's accuracy (UA) across various algorithms.

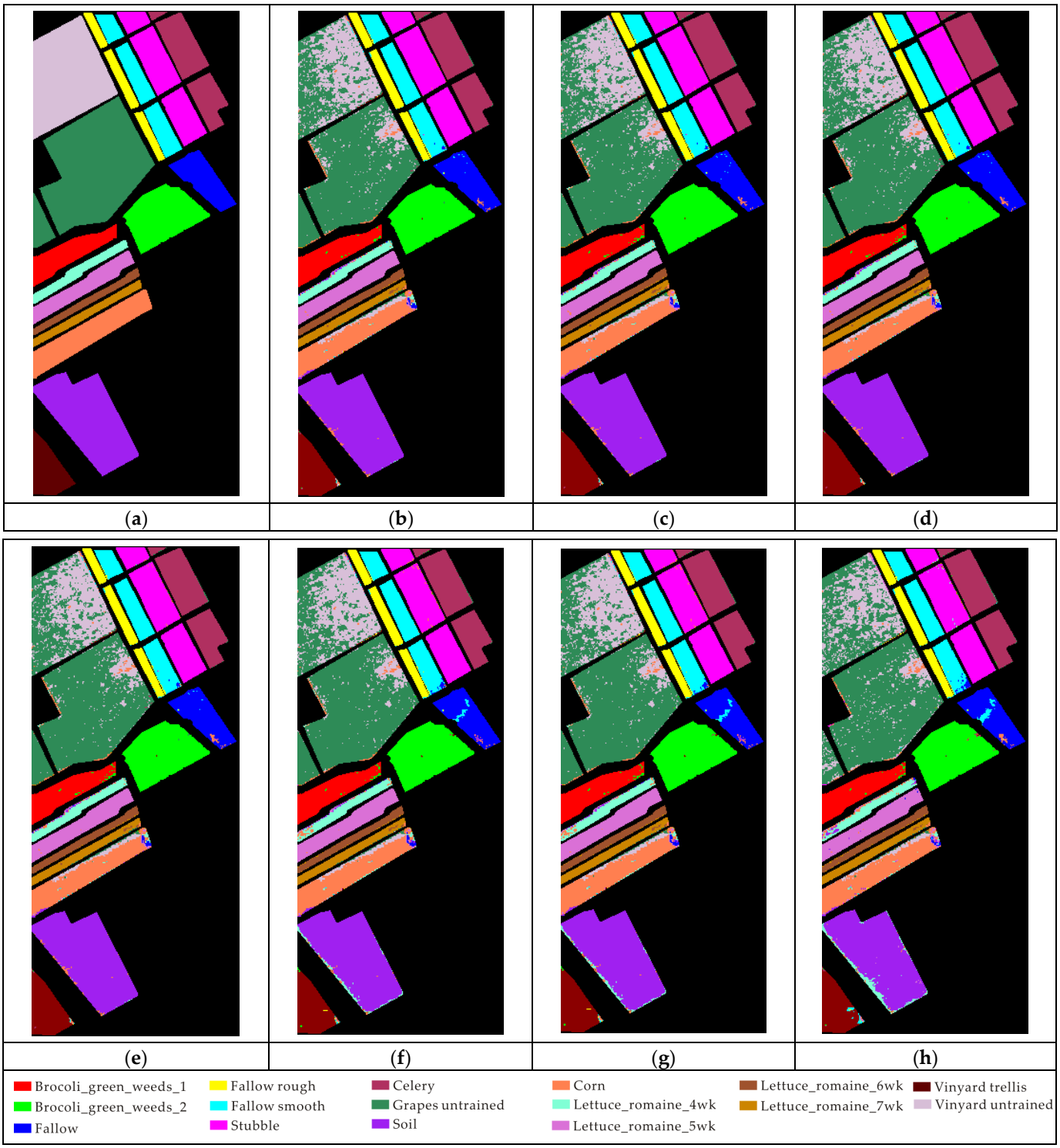


Figure 7. Crop identification and mapping images of Salinas Valley data set. (**a**) The ground truth; (**b**) the proposed CS-AP method; (**c**) the SS-AP method; (**d**) the LSBS method; (**e**) the FM-AP method; (**f**) the ED-AP method; (**g**) the MVPCA method; (**h**) the baseline with 204 bands.

Broccoli_green_weeds_1 achieved 100% UA with the MVPCA, ED-AP, FM-AP, LSBS, and CS-AP methods, while the baseline and SS-AP methods reached 99.70% and 99.85%, respectively. This indicates minimal misclassification between similar crop categories. For broccoli_green_feeds_2, the UA decreased slightly by 2–3%, but both PA and UA remained high, indicating satisfactory classification. The fallow, divided into three types (fallow, fallow rough, and fallow smooth), also showed strong spectral similarity. Fallow

rough had the fewest misclassifications, while fallow and fallow smooth were occasionally misclassified due to mixed features. All methods yielded PA and UA above 90%, with fallow rough achieving the highest PA (above 97%). Stubble showed 100% UA with all methods, except MVPCA and ED-AP, which achieved 99.64% and 99.67%, respectively. For celery, PA and UA were greater than 98%, with only a few misclassified pixels as grapes untrained. Untrained grapes and untrained vineyards had highly similar spectral features, resulting in UA values between 67.48% and 74.15%. Vineyard trellises had high PA and UA (95.40% to 99.16%), with no significant confusion with untrained vineyards due to better spectral distinction. Soil had PA and UA greater than 92.65% and 97.37%, respectively.

A few pixels were misclassified as fallow smooth with ED-AP, MVPCA, and the baseline and as stubble with the CS-AP, SS-AP, LSBS, and FM-AP methods. Corn had the worst classification performance with PA ranging from 75.46% to 76.55% and UA from 78.50% to 81.27%. However, the CS-AP method achieved the highest values, indicating its strong performance in crop recognition. Corn was often misclassified strained vineyard. Romaine lettuce (classified by the following growth stages: 4-week, 5-week, 6-week, and 7-week) showed a strong correlation across stages. The 5-week, 6-week, and 7-week stages had PA and UA above 88.95%, while 4-week had lower values (PA: 79.31–82.08%; UA: 65.94–67.98%). The CS-AP, LSBS, and SS-AP methods achieved values above 93%, highlighting the ability to classify crops at different growth stages using remote sensing.

Table 4 presents the classification accuracies achieved for the Indian Pines 92AV3C data set with varying numbers of selected bands. Figure 8 shows the crop identification and mapping images. The proposed CS-AP method achieves the highest accuracies on the Indian Pines 92AV3C data set compared to all other methods when using 50 bands. Specifically, the OA obtained with CS-AP is +2.11% higher than the baseline. A similar trend is observed when comparing CS-AP to MVPCA, ED-AP, FM-AP, LSBS, and SS-AP. The optimal number of selected bands for each method varies: MVPCA and FM-AP achieve their best performance with 60 bands, ED-AP and LSBS with 55 bands, and SS-AP with 50 bands. Notably, CS-AP also selects 50 bands, the same as SS-AP, yet it delivers superior OA while requiring fewer bands compared to several other methods.

The proposed CS-AP method outperforms other methods in classifying oats, achieving the highest PA, 23.79% higher than the MVPCA and ED-AP methods. Notably, these two methods had the lowest PA (<6%) for oats, but oats achieved the highest UA, with 100% for all methods except ED-AP (75%). The classification of building–grass–trees–drives was less satisfactory, with PA ranging from 43.21% to 59.88% and the highest value achieved via CS-AP. The UA for this class was around 60%, indicating confusion with woods, grass–trees, and soybeans—minimum-till. Corn, divided into corn, corn—minimum-till, and corn—no-till, showed high confusion between types due to spectral similarities. The MVPCA method had the lowest PA (37.19%, 50.98%, and 56.02%). Grass was divided into grass—pasture—mowed, grass—pasture, and grass—trees. The PA for grass—pasture-mowed was the lowest (63.58–75.68%) using various methods, but CS-AP achieved 88.94%, about 15 percentage points higher than the others. Grass—pasture and grass—trees had satisfactory results with PA higher than 72.73% and 89.80%, respectively. Soybeans—minimum had a wide distribution and PA and UA greater than 75.27% and 69.26%. CS-AP achieved the highest UA, improving misclassification. Soybeans—clean till had poor classification performance (PA between 46.08% and 60.34%), while soybeans—no till performed better (PA > 67.39%, but not higher than 77%). Stone–steel–tower achieved 100% UA except for MVPCA, with PA higher than 80%. Wheat and woods also showed strong separability, with PA > 95.58% and 94.53%, and UA > 82.24% and 92.80%, respectively.

Table 4. PA, UA, and OA metrics achieved with the baseline, MVPAC, ED-AP, FM-AP, LSBS, SS-AP (NCS = 105 with k = 150), and proposed CS-AP (NCS = 99) methods were evaluated for different numbers of selected bands on the Indian Pines 92AV3C data set.

Class and Accuracy		NB	Baseline	NB	MVPCA	NB	ED-AP	NB	FM-AP	NB	LSBS	NB	SS-AP	NB	CS-AP
Alfalfa	PA (%)		76.92		44.68		65.96		78.72		**78.75**		72.34		74.47
	UA (%)		63.83		71.30		65.78		**74.00**		71.15		70.83		72.92
Building–grass–trees–Drives	PA (%)		52.81		45.67		58.64		43.21		57.10		50.93		**59.88**
	UA (%)		63.80		**78.54**		66.20		61.40		60.25		63.22		63.36
Corn	PA (%)		67.07		37.19		57.29		**70.85**		62.31		70.35		69.85
	UA (%)		65.09		53.62		65.52		**66.51**		65.61		62.78		64.95
Corn—minimum till	PA (%)		54.48		50.98		56.02		**60.78**		54.76		59.94		58.26
	UA (%)		61.10		59.48		61.92		68.13		67.30		**68.92**		68.31
Corn—no till	PA (%)		71.47		56.02		71.06		68.05		72.52		71.22		**72.73**
	UA (%)		73.13		62.86		**73.38**		69.12		72.64		72.22		68.49
Grass—pasture	PA (%)		83.33		72.73		72.73		86.36		86.34		86.36		**86.38**
	UA (%)		75.00		**100.00**		72.73		82.61		67.86		79.17		67.86
Grass—pasture—mowed	PA (%)		63.58		63.79		72.24		64.37		75.68		68.80		**88.94**
	UA (%)	200	89.12	60	90.56	55	89.63	60	92.25	**55**	**93.62**	50	88.05	50	91.41
Grass—trees	PA (%)		91.22		**98.00**		93.25		92.15		89.80		90.11		90.42
	UA (%)		72.98		74.97		77.65		71.50		83.99		75.13		**86.62**
Hay—windrowed	PA (%)		97.08		98.80		97.36		97.84		98.80		97.84		**98.88**
	UA (%)		**96.79**		87.63		94.85		95.09		96.23		95.99		96.23
Oats	PA (%)		14.29		5.88		17.65		29.41		5.88		23.53		**29.67**
	UA (%)		**100.00**		**100.00**		75.00		**100.00**		**100.00**		**100.00**		**100.00**
Soybeans—clean till	PA (%)		53.13		49.14		46.08		60.23		54.68		59.27		**60.34**
	UA (%)		71.56		43.34		50.21		**77.97**		56.19		77.13		75.85
Soybeans—minimum	PA (%)		**77.60**		76.06		76.42		77.18		75.27		77.42		76.61
	UA (%)		74.17		69.26		71.96		75.67		73.69		75.62		**75.63**
Soybeans—no till	PA (%)		72.87		67.39		67.63		76.09		72.10		**76.21**		75.36
	UA (%)		63.96		69.32		**66.43**		65.28		64.19		64.98		65.55
Stone–steel–tower	PA (%)		81.08		80.00		82.22		83.33		81.11		83.33		**83.47**
	UA (%)		**100.00**		97.30		**100.00**		**100.00**		**100.00**		**100.00**		**100.00**
Wheat	PA (%)		98.66		98.33		95.58		97.79		97.79		**99.45**		97.24
	UA (%)		83.52		**94.65**		87.37		80.82		82.33		83.72		82.24
Woods	PA (%)		94.53		**96.97**		95.33		95.42		95.69		95.24		95.33
	UA (%)		92.80		**98.60**		93.73		92.83		93.34		93.31		93.65
OA (%)			75.57		72.57		74.98		76.27		76.01		76.95		**77.68**

The bold entries in Table 4 represent the highest values for the producer's accuracy (PA) and the user's accuracy (UA) across various algorithms.

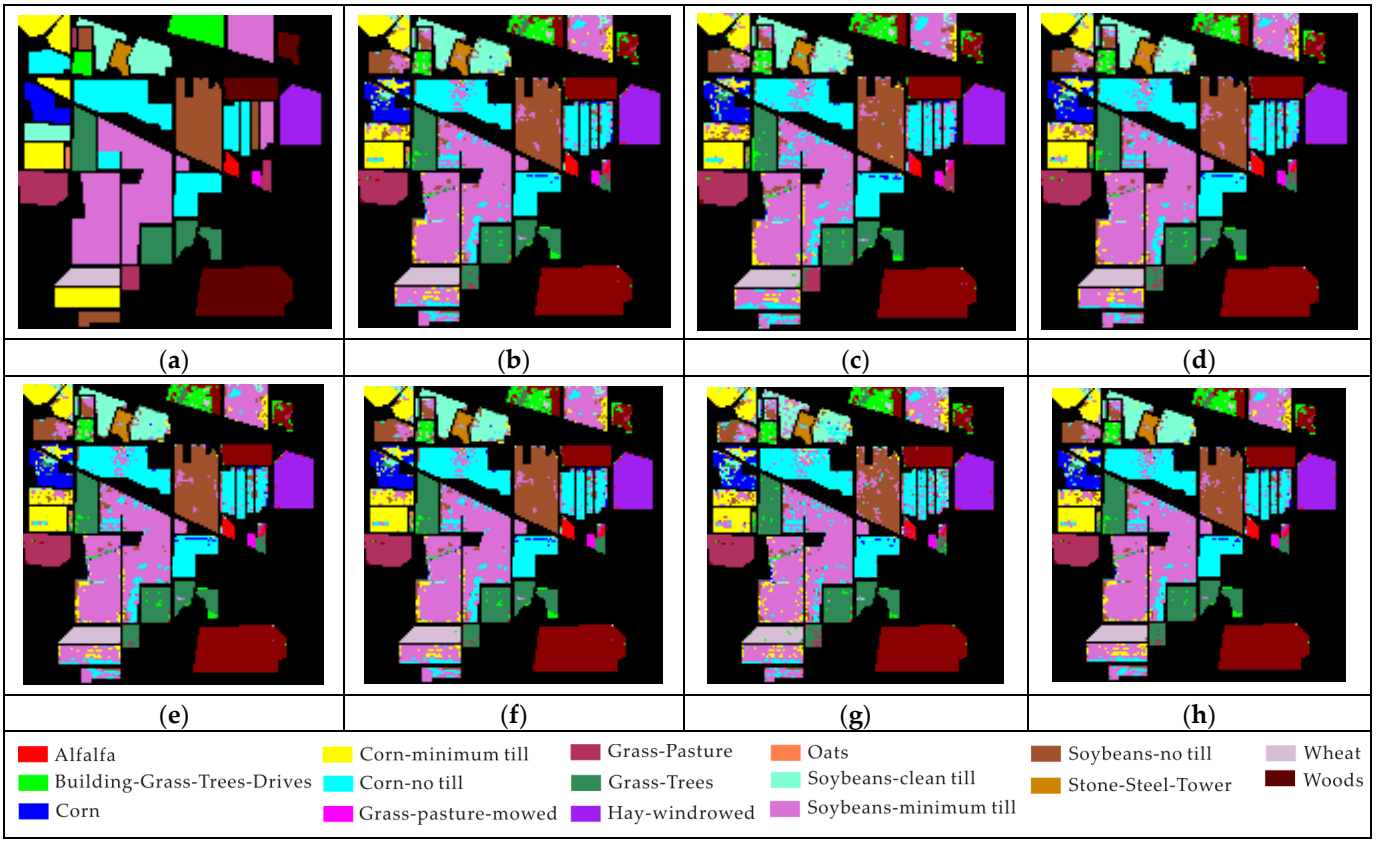


Figure 8. Crop identification and mapping images of Indian Pines 92AV3C data set. (**a**) The ground truth; (**b**) the proposed CS-AP method; (**c**) the SS-AP method; (**d**) the LSBS method; (**e**) the FM-AP method; (**f**) the ED-AP method; (**g**) the MVPCA method; (**h**) the baseline with 200 bands.

3.3.4. Parameter Sensitivity Analysis

The proposed CS-AP method has two hyper-parameters:

- k, which determines the NCS number;
- CTS_{CS}, which controls the quantity of selected bands used for crop identification and classification.

The k hyper-parameter can take any positive value, with different k values leading to varying numbers of NCSs. A larger k value results in a greater number of larger NCSs. For HSIs, the value of k should be chosen based on the image size. For larger HSIs, a higher k value is necessary because a smaller k value would produce fewer and overly large superpixels, which can lead to the misclassification of crops. Conversely, for smaller HSIs, excessively high k values could lead to very small superpixels, which may also impair classification accuracy due to spatial distance calculations in SLIC the superpixels algorithm. In the experiments, the hyper-parameter k values were set to 100, 300, 500, 700, and 900 for the Salinas Valley data set, resulting in 119, 285, 502, 643, and 708 NCS, respectively. For the Indian Pines 92AV3C data set, the hyper-parameter k values were set to 50, 100, 150, 200, and 300, corresponding to 53, 83, 99, 113, and 121 NCS, respectively. For the CTS_{CS} hyper-parameter, higher values result in fewer selected bands. The CTS_{CS} value should be set according to the desired number of selected bands, as illustrated in Figure 9.

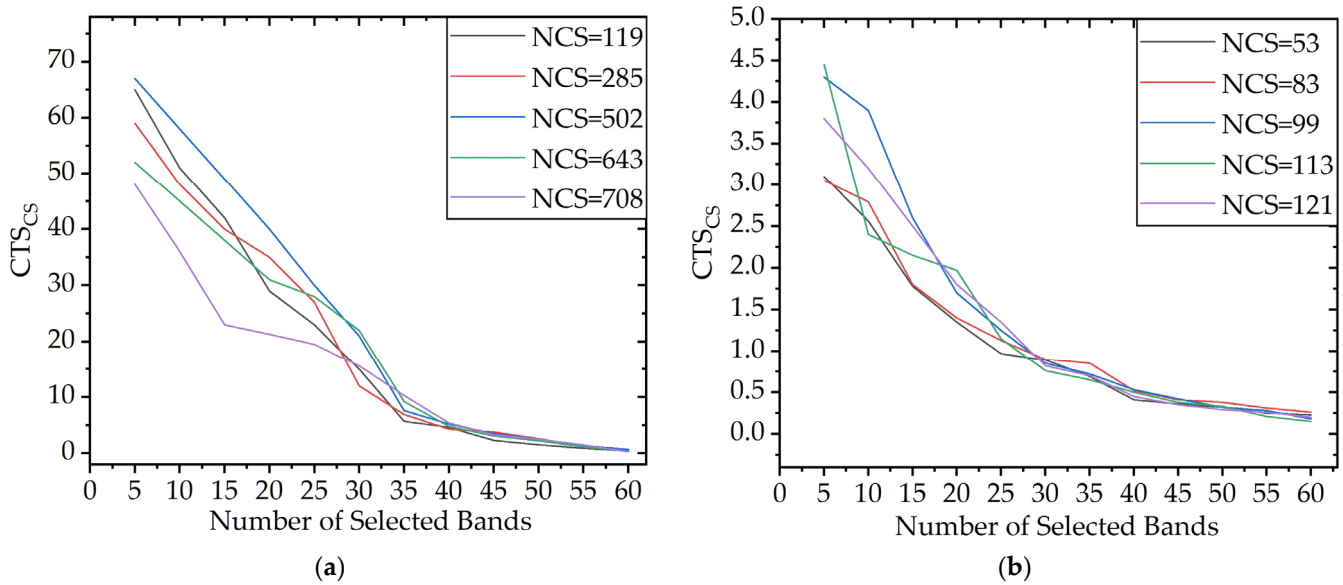


Figure 9. The value of the CTScs parameter versus the number of selected bands for the proposed CS-AP with a varying number of crop superpixels: (**a**) Salinas Valley data set; (**b**) Indian Pines 92AV3C data set.

4. Discussion

From the experimental results presented in the previous section, it is evident that the proposed CS-AP method consistently outperforms other band selection methods in terms of OA, PA, and UA across the data sets considered. This section focuses on discussing the effectiveness of band selection algorithms in relation to crop superpixels, selection methods, crop identification, and mapping.

4.1. Band Selection Performance Compared to Different Crop Superpixels

The OA of the CS-AP method demonstrates distinct trends with varying numbers of CSs in Figure 4, revealing differences in performance compared to the baseline.

The results of crop identification and classification demonstrate that the proposed CS-AP method demonstrated a higher OA compared to the baseline, even when fewer bands were selected, across all five different CSs on the two data sets. Specifically, for the Salinas Valley data set, the CS-AP method outperformed the baseline using all 204 channels when we selected over 40 bands. The highest OA was achieved with 45 bands and a CS value of 643. However, when the number of selected bands varied between 15 and 30, the OA values were comparable to or slightly better than the baseline but exhibited significant fluctuations. Notably, a pronounced drop in OA was observed when selecting 30 bands. For the Indian Pines 92AV3C data set, most OA surpassed the baseline (utilizing all 200 channels) when 30 bands were selected. However, the OA varied considerably, depending on the CSs used. The best performance was achieved with a CS value of 99. Based on these findings, the subsequent experiments used a CS value of 643 for the Salinas Valley data set and 99 for the Indian Pines 92AV3C data set.

4.2. Band Selection Performance Compared to Different Methods

For the Salinas Valley data set, the CS-AP method demonstrated the best performance, achieving an overall accuracy (OA) of 88.13% with 45 bands selected and outperforming the baseline (87.17%). While the SS-AP and LSBS methods showed comparable or slightly better results when fewer bands were selected, the CS-AP method remained the top performer when 45 bands were chosen. The MVPCA and ED-AP methods consistently underperformed, especially with fewer bands, failing to surpass the baseline even with

more bands selected. The spectral selection of CS-AP was more targeted, capturing important absorption features, while other methods (such as SS-AP and FM-AP) had limitations in capturing key bands or exhibited redundancy.

For the Indian Pines data set, the CS-AP method also outperformed the baseline with an OA of 77.68% when 25 bands were selected, surpassing the baseline (75.57%). The SS-AP method showed competitive performance but was slightly lower or on par with CS-AP. The MVPCA and ED-AP methods continued to underperform, while the FM-AP and LSBS methods performed below the baseline with fewer than 25 bands but matched or exceeded it when more than 35 bands were selected. The CS-AP method demonstrated better spectral feature selection, covering both strong and moderate absorption features, while other methods like FM-AP had more concentrated selections with gaps in critical spectral regions.

4.3. Crop Identification and Mapping

For the Salinas Valley data set, most crops achieved high UA and PA values. Broccoli_green_feeds_1 and broccoli_green_feeds_2 showed high classification accuracy. The fallow categories had good classification results, with fallow rough showing the least misclassification and all categories achieving PA and UA above 90%. Stubble also achieved 100% UA with all methods. Celery had PA and UA greater than 98%, with only slight misclassification as grapes untrained. Corn had the lowest classification performance, with PA ranging from 75.46% to 76.55% and UA from 78.50% to 81.27%, but the CS-AP method achieved the highest accuracy. Romaine lettuce romaine at different growth stages and showed good classification results, with PA and UA above 88.95% for the 5-week, 6-week, and 7-week stages, but the 4-week stage had lower values. Therefore, the CS-AP method proved to be highly effective for crop identification and mapping in the Salinas Valley data set, with many crops showing high classification accuracy, especially those with distinct spectral features like broccoli_green_weeds_1 and stubble. However, crops with similar spectral signatures, such as the different types of fallow and corn, present challenges, resulting in some misclassifications. The classification accuracy varies, depending on crop growth stages, with mature crops being easier to distinguish. The proposed CS-AP method outperforms others, especially for challenging crops. Despite the promising results, further improvements in algorithms, particularly for spectrally similar crops and early growth stages, are needed for more accurate and reliable crop mapping in precision agriculture.

For the Indian Pines 92AV3C data set, the proposed CS-AP method outperformed other methods in classifying crops and achieving the highest classification accuracy for oats, grass—pasture-mowed, and stone–steel–tower. It also improved classification for the soybeans—minimum, corn, and grass types. For crops like building–grass–trees–drives and soybeans—clean till, the CS-AP method provided better results compared to other methods. It achieved higher accuracy in both user and producer accuracy, especially for crops like oats and grass—pasture-mowed, where other methods struggled. Despite some confusion between similar crop types (e.g., corn variants and soybean types), the CS-AP method generally yields higher accuracy, especially in cases with spectral similarity. Overall, the CS-AP method shows strong performance in distinguishing crop types and minimizing misclassifications. It can enhance crop identification and mapping by providing more accurate results, making it a valuable tool for precision agriculture and land management.

5. Conclusions

In this study, a CS-AP band selection method has been proposed for crop identification and mapping. Given spatial regional characteristics and the spectral variability of different crops or the same crop in different growth cycles, a new type of the most informative

structure, i.e., CSs, was generated based on the PCA and SLIC superpixel algorithm. Next, a series of optimal crop identification bands were obtained according to the RCA with AP to measure the identification and classification capability of spectral bands.

The performance of all crop categories and the proposed CS-AP method were analyzed on two ideal agricultural AVIRIS data sets, i.e., Salinas Valley, California, USA, and Indian Pines 92AV3C over northwest Indiana. Compared with using all bands (204 bands on the Salinas Valley data set and 200 bands on the Indian Pines 92AV3C data set), two unsupervised band selection methods (i.e., the MVPCA and the ED-AP method) and three semi-supervised band selection methods (i.e., the FM-AP, the LSBS, and the SS-AP method), the proposed CS-AP method can achieve the best identification and classification accuracy and performance with a relatively lower number of bands (45 bands for the Salinas Valley data set and 50 bands for the Indian Pines 92AV3C data set).

In future work, some distance constraints will be introduced between different types of crops to structure a new crop superpixel space for further improving the crop identification and classification results.

Author Contributions: Conceptualization, Y.T.; methodology, Y.T., J.G. and L.L.; validation, Y.T., Y.C. and J.G.; formal analysis, Y.T., Y.L. and J.H.; investigation, Y.T. and Y.W.; data curation, Y.T., L.Z. and L.P.; writing—original draft preparation, Y.T.; writing—review and editing, Y.T. and Y.C.; visualization, Y.W. and J.G.; supervision, L.Z. and L.L.; All authors have read and agreed to the published version of the manuscript.

Funding: This research was funded by Jilin Province Natural Science Foundation, grant number 20230101311JC, the National Science and Technology Major Project, grant number 2024ZD1001000, the Jilin Provincial Department of Education Excellent Youth Project, grant number JJKH20240783KJ, and the National Natural Science Foundation of China, grant number 42272340 and 42241163.

Data Availability Statement: The original contributions presented in the study are included in the article, further inquiries can be directed to the corresponding author.

Acknowledgments: The authors would like to express their sincere gratitude to the editors and anonymous reviewers for their time and invaluable efforts in reviewing this manuscript.

Conflicts of Interest: The authors declare no conflicts of interest.

References

1. Smith, R.B. *Introduction to Hyperspectral Imaging*; TNTmips; Micro Images: Lincoln, NE, USA, 2012; pp. 1–24.
2. Inbal, R.; Ran, N.L.; Fadi, K. Weed species identification: Acquisition, feature analysis, and evaluation of a hyperspectral and RGB dataset with labeled data. *Remote Sens.* **2024**, *16*, 2808. [CrossRef]
3. Liang, L.; Di, L.P.; Zhang, L.P.; Deng, M.X.; Qin, Z.H.; Zhao, S.H.; Lin, H. Estimation of crop LAI using hyperspectral vegetation indices and a hybrid inversion method. *Remote Sens. Environ.* **2015**, *165*, 123–134. [CrossRef]
4. Mirzaei, S.; Pascucci, S.; Carfora, M.F.; Casa, R.; Rossi, F.; Santini, F.; Palombo, F.; Laneve, G.; Pignatti, S. Early-season crop mapping by PRISMA images using machine/deep learning approaches: Italy and Iran test cases. *Remote Sens.* **2024**, *16*, 2431. [CrossRef]
5. Guo, H.L.; Zhang, R.R.; Dai, W.H.; Zhou, X.W.; Zhang, D.J.; Yang, Y.H.; Cui, J. Mapping soil organic matter content based on feature band selection with zy1-02d hyperspectral satellite data in the agricultural region. *Agronomy* **2022**, *12*, 2111. [CrossRef]
6. Prabhakar, M.; Gopinath, K.A.; Kumar, N.P.; Thirupathi, M.; Sravan, U.S.; Kumar, G.S.; Siva, G.S.; Chandana, P.; Singh, V.K. mapping leaf area index at various rice growth stages in southern india using airborne hyperspectral remote sensing. *Remote Sens.* **2024**, *16*, 954. [CrossRef]
7. Ma, H.; Zhao, K.X.; Jin, X.; Ji, J.T.; Qiu, Z.M.; Gao, S. Spectral difference analysis and identification of different maturity blueberry fruit based on hyperspectral imaging using spectral index. *Int. J. Agric. Biol. Eng.* **2019**, *12*, 134–140. [CrossRef]
8. Guo, Y.H.; Xiao, Y.; Hao, F.H.; Zhang, X.; Chen, J.H.; Beurs, B.D.; He, Y.H.; Fu, Y.H. Comparison of different machine learning algorithms for predicting maize grain yield using UAV-based hyperspectral images. *Int. J. Appl. Earth Obs.* **2023**, *124*, 103528. [CrossRef]
9. Hughes, G. On the mean accuracy of statistical pattern recognizers. *IEEE Trans. Inf. Theory* **1968**, *14*, 55–63. [CrossRef]

10. Bruzzone, L.; Demir, B. A review of modern approaches to classification of remote sensing data. In *Land Use and Land Cover Mapping in Europe*; Springer: Dordrecht, The Netherlands, 2014; Volume 18, pp. 127–143.
11. Plaza, A.; Benediktsson, J.A.; Boardman, J.W.; Brazile, J.; Bruzzone, L.; Camps-Valls, G.; Chanussot, J.; Fauvel, M.; Gamba, P.; Gualtieri, A. Recent advances in techniques for hyperspectral image processing. *Remote Sens. Environ.* **2009**, *113*, S110–S122. [CrossRef]
12. Md, R.I.; Ayasha, S.; Masud, I.A.; Md, P.U.; Anwaar, U. Hyperspectral image classification via information theoretic dimension reduction. *Remote Sens.* **2023**, *15*, 1147. [CrossRef]
13. Dave, K.; Vyas, T.; Trivedi, Y.N. A sample selection method based on similarity measure and fuzziness for crop classification from hyperspectral data. *Adv. Space Res.* **2024**, *73*, 1262–1268. [CrossRef]
14. Shi, Y.T.; Fu, B.; Wang, N.; Cheng, Y.Z.; Fang, J.; Liu, X.B.; Zhang, G. Spectral-spatial attention rotation-invariant classification network for airborne hyperspectral images. *Drones* **2023**, *7*, 240. [CrossRef]
15. Yang, H.; Chen, M.; Wu, G.W.; Wang, J.L.; Wang, Y.X.; Hong, Z.H. Double deep Q-network for hyperspectral image band selection in land cover classification applications. *Remote Sens.* **2023**, *15*, 682. [CrossRef]
16. Wei, Y.P.; Hu, H.Q.; Xu, H.X.; Mao, X.B. Unsupervised hyperspectral band selection via multimodal evolutionary algorithm and subspace decomposition. *Sensors* **2023**, *23*, 2129. [CrossRef] [PubMed]
17. Pan, X.; Zhang, S. Parallelized remote sensing classifier based on rough set theory algorithm. In Proceedings of the 2012 20th International Conference on Geoinformatics, Hong Kong, China, 15–17 June 2012.
18. Moharram, M.A.; Sundaram, D.M. Mayfly algorithm-based semi-supervised band selection with enhanced bitonic filter for spectral-spatial hyperspectral image classification. *Int. J. Remote Sens.* **2024**, *45*, 2073–2108. [CrossRef]
19. Sun, K.; Geng, X.; Ji, L.; Lu, Y. A new band selection method for hyperspectral image based on data quality. *IEEE J. Sel. Top. Appl. Earth Obs. Remote Sens.* **2014**, *7*, 2697–2703. [CrossRef]
20. Ren, Z.L.; Zhai, Q.P.; Sun, L. A novel method for hyperspectral mineral mapping based on clustering-matching and nonnegative matrix factorization. *Remote Sens.* **2022**, *14*, 1042. [CrossRef]
21. Chang, C.I.; Du, Q.; Sun, T.L.; Althouse, M.L.G. A joint band prioritization and band-decorrelation approach to band selection for hyperspectral image classification. *IEEE Trans. Geosci. Remote Sens.* **1999**, *37*, 2631–2641. [CrossRef]
22. Eckel, L.; Stütz, P. Hyperspectral sensor management for uas: Sensor context based band selection for anomaly detection. In Proceedings of the IEEE Aerospace Conference, Big Sky, MT, USA, 2–9 March 2024.
23. Cover, T.M.; Thomas, J.A. *Elements of Information Theory*, 2nd ed.; Wiley: New York, NY, USA, 2006.
24. Arzuaga, C.E.; Jimenez, R.L.O.; Velez, R.M. Unsupervised feature extraction and band subset selection techniques based on relative entropy criteria for hyperspectral data analysis. In Proceedings of the 2003 Conference on Algorithms and Technologies for Multispectral, Hyperspectral, and Ultraspectral Imagery IX, Orlando, FL, USA, 21–24 April 2003.
25. Chaudhri, S.N.; Roy, S.K. A discriminatory groups-based supervised band selection technique for hyperspectral image classification. *Remote Sens. Lett.* **2024**, *15*, 111–120. [CrossRef]
26. Sugiyama, M. Dimensionality reduction of multimodal labeled data by local fisher discriminant analysis. *J. Mach. Learn. Res.* **2007**, *8*, 1027–1061.
27. Shao, H.; Li, X.Y.; Sun, L.; Wang, C.; Hu, Y.X. A hyperspectral band selection algorithm for identifying high oleic acid peanuts. *J. Near Infrared. Spec.* **2024**, *32*, 10–17. [CrossRef]
28. Jarocinska, A.; Kopec, D.; Kycko, M.; Piorkówsk, H.; Blonska, A. Hyperspectral vs. multispectral data: Comparison of the spectral differentiation capabilities of Natura 2000 non-forest habitats. *ISPRS J. Photogramm. Remote Sens.* **2022**, *184*, 148–164. [CrossRef]
29. Aravinth, J.; Veni, S.; Dheepika, R.; Polamuri, V.G.; Poornima, A.R.; Sandeep, K.S. Optimal hyperspectral band selection using robust multi-verse optimization algorithm. *Multimed. Tools Appl.* **2023**, *82*, 14663–14687.
30. Shi, J.; Zhang, X.; Liu, X.D.; Lei, Y.; Jeon, W. Multicriteria semi-supervised hyperspectral band selection based on evolutionary multitask optimization. *Knowl.-Based Syst.* **2022**, *240*, 107934. [CrossRef]
31. G Camps-Valls, G.; Bruzzone, L. Kernel-based methods for hyperspectral image classification. *IEEE Trans. Geosci. Remote Sens.* **2005**, *43*, 1351–1362. [CrossRef]
32. Zhang, Y.Q.; Cao, G.; Li, X.S.; Wang, B.S.; Fu, P. Active semi-supervised random forest for hyperspectral image classification. *Remote Sens.* **2019**, *11*, 2974. [CrossRef]
33. Darvishzadeh, R.; Atzberger, C.; Skidmore, A.; Schlerf, M. Mapping grassland leaf area index with airborne hyperspectral imagery: A comparison study of statistical approaches and inversion of radiative transfer models. *ISPRS J. Photogramm. Remote Sens. Remote Sens.* **2011**, *66*, 894–906. [CrossRef]
34. Sarma, A.S.; Nidamanuri, B.R. Evolutionary optimisation techniques for band selection in drone-based hyperspectral images for vegetable crops mapping. In Proceedings of the IEEE International Geoscience and Remote Sensing Symposium (IGARSS), Pasadena, CA, USA, 16–21 July 2023.
35. Agilandeeswari, L.; Prabukumar, M.; Radhesyam, V.; Phaneendra, K.L.N.B.; Farhan, A. Crop classification for agricultural applications in hyperspectral remote sensing images. *Appl. Sci.* **2022**, *12*, 1670. [CrossRef]

36. Rabi, N.S.; Shalini, G.; Rajan, G.R.; Jochem, V.; Rajeev, R.; Tarun, K.; Mahesh, C.M.; Joydeep, M.; Anchal, D.; Sudhir, K.; et al. optimizing the retrieval of wheat crop traits from uav-borne hyperspectral image with radiative transfer modelling using gaussian process regression. *Remote Sens.* **2023**, *15*, 5496. [CrossRef]
37. Zhang, Y.; Hui, J.; Qin, Q.M.; Sun, Y.H.; Zhang, T.Y.; Sun, H.; Li, M.Z. Transfer-learning-based approach for leaf chlorophyll content estimation of winter wheat from hyperspectral data. *Remote Sens. Environ.* **2021**, *267*, 112724. [CrossRef]
38. Kang, Y.M.; Ye, P.S.; Bai, Y.X.; Qiu, S. Hyperspectral image based interpretable feature clustering algorithm. *Comput. Mater. Contin.* **2024**, *79*, 2151–2168. [CrossRef]
39. Cheng, E.H.; Wang, F.M.; Peng, D.L.; Zhang, B.; Zhao, B.; Zhang, W.J.; Hu, J.K.; Lou, Z.H.; Yang, S.L.; Zhang, H.C.; et al. A GT-LSTM spatio-temporal approach for winter wheat yield prediction: From the field scale to county scale. *IEEE Trans. Geosci. Remote Sens.* **2024**, *62*, 4409318. [CrossRef]
40. Frey, J.F.; Dueck, D. Clustering by passing messages between data points. *Science* **2007**, *315*, 972–976. [CrossRef]
41. Yang, C.; Tan, Y.L.; Bruzzone, L.; Lu, L.J.; Guan, R.C. Discriminative feature metric learning in the affinity propagation model for band selection in Hyperspectral images. *Remote Sens.* **2017**, *9*, 782. [CrossRef]
42. Su, H.J.; Sheng, Y.H.; Du, P.J.; Liu, K. Adaptive affinity propagation with spectral angle mapper for semi-supervised hyperspectral band selection. *Appl. Optics.* **2012**, *51*, 2656–2663. [CrossRef]
43. Qian, Y.; Yao, F.; Jia, S. Band selection for hyperspectral imagery using affinity propagation. *IET Comput. Vis.* **2009**, *3*, 213–222. [CrossRef]
44. Yang, C.; Liu, S.; Bruzzone, L.; Guan, R.C. A semisupervised feature metric based band selection method for hyperspectral image classification. In Proceedings of the 4th Workshop on Hyperspectral Image and Signal Processing: Evolution in Remote Sensing, Shanghai, China, 4–7 July 2012; pp. 1–4.
45. Yang, C.; Liu, S.C.; Bruzzone, L.; Guan, R.C.; Du, P.J. A feature-metric-based affinity propagation technique to feature selection for Hyperspectral Image Classification. *IEEE Geosci. Remote Sens. Lett.* **2013**, *10*, 1152–1156. [CrossRef]
46. Csillik, O. Fast segmentation and classification of very high resolution remote sensing data using SLIC superpixels. *Remote Sen.* **2017**, *9*, 243. [CrossRef]
47. Achanta, R.; Shaji, A.; Smith, K.; Lucchi, A.; Fua, P.; Süsstrunk, S. SLIC superpixels compared to state-of-the-art superpixel methods. *IEEE T. Pattern Anal.* **2012**, *34*, 2274–2282. [CrossRef]
48. Liao, N.N.; Gong, J.L.; Li, W.X.; Li, C.; Zhang, C.Y.; Guo, B.L. SMALE: Hyperspectral image classification via superpixels and manifold learning. *Remote Sens.* **2024**, *16*, 3442. [CrossRef]
49. Tang, C.; Wang, J.; Zheng, X.; Liu, X.W.; Xie, W.Y.; Li, X.J.; Zhu, X.Z. Spatial and spectral structure preserved self-representation for unsupervised hyperspectral band selection. *IEEE Trans. Geosci. Remote Sens.* **2023**, *61*, 5531413. [CrossRef]
50. Tan, Y.L.; Lu, L.J.; Bruzzone, L.; Guan, R.C.; Chang, Z.Y.; Yang, C. Hyperspectral band selection for lithologic discrimination and geological mapping. *IEEE J. Sel. Top. Appl. Earth Obs. Remote Sens.* **2020**, *13*, 471–486. [CrossRef]
51. Yang, C.; Bruzzone, L.; Zhao, H.S.; Tan, Y.L.; Guan, R.C. Superpixel-based unsupervised band selection for classification of Hyperspectral images. *IEEE Trans. Geosci. Remote Sens.* **2018**, *56*, 1–16. [CrossRef]
52. Pochamreddy, P.; Alkhatib, M.Q.; Velez-Reyes, M. Evaluating the effect of band subset selection in SLIC superpixel segmentation. In *Algorithms, Technologies, and Applications for Multispectral and Hyperspectral Imagery XXVI*; Electr Network; SPIE: Bellingham, WA, USA, 2020.
53. Bro, R.; Smilde, A.K. Principal component analysis. *Anal. Methods* **2014**, *6*, 2812–2831. [CrossRef]
54. Bar-Hillel, A.; Hertz, T.; Shental, N.; Weinshall, D. Learning distance functions using equivalence relations. In Proceedings of the 20th International Conference on Machine Learning (ICML-03), Washington, DC, USA, 21–24 August 2003.
55. Bar-Hillel, A.; Hertz, T.; Shental, N.; Weinshall, D. Learning a Mahalanobis metric from equivalence constraints. *J. Mach. Learn. Res.* **2005**, *6*, 937–965.
56. Mika, S.; Ratsch, G.; Weston, J.; Scholkopf, B.; Muller, K. Fisher discriminant analysis with kernels. In Proceedings of the IEEE Signal Processing Society Workshop, Madison, WI, USA, 25 August 1999.
57. Li, W.; Prasad, S.; Fowler, J.E.; Bruce, L.M. Locality-preserving dimensionality reduction and classification for hyperspectral image analysis. *IEEE Trans. Geosci. Remote Sens.* **2012**, *50*, 1185–1198. [CrossRef]
58. Hyperspectral Remote Sensing Scenes. Available online: http://www.ehu.eus/ccwintco/index.php/Hyperspectral_Remote_Sensing_Scenes (accessed on 14 December 2021).
59. Boggavarapu, L.N.P.K.; Manoharan, P. Classification of Hyper Spectral Remote Sensing Imagery Using Intrinsic Parameter Estimation. In Proceedings of the ISDA 2018: International Conference on Intelligent Systems Design and Applications, Vellore, India, 6–8 December 2018.
60. Boggavarapu, L.N.P.K.; Manoharan, P. Whale optimization-based band selection technique for hyperspectral image classification. *Int. J. Remote Sens.* **2021**, *42*, 5105–5143.

61. Boggavarapu, L.N.P.K.; Manoharan, P. Survey on classification methods for hyper spectral remote sensing imagery. In Proceedings of the 2017 International Conference on Intelligent Computing and Control Systems (ICICCS), Madurai, India, 15–16 June 2017; pp. 538–542.
62. Baisantry, M.; Sao, A.K.; Shukla, D.P. Two-Level Band Selection Framework for Hyperspectral Image Classification. *J. Indian Soc. Remote Sens.* **2021**, *49*, 843–856. [CrossRef]
63. Vaddi, R.; Manoharan, P. Hyperspectral image classification using CNN with spectral and spatial features integration. *Infrared Phys. Techn.* **2020**, *107*, 103296. [CrossRef]
64. Boggavarapu, L.N.P.K.; Manoharan, P. Hyperspectral image classification using fuzzy-embedded hyperbolic sigmoid nonlinear principal component and weighted least squares approach. *J. Appl. Remote Sens.* **2020**, *14*, 024501.
65. Boggavarapu, L.N.P.K.; Manoharan, P. A new framework for hyperspectral image classification using Gabor embedded patch based convolution neural network. *Infrared Phys. Techn.* **2020**, *110*, 103455. [CrossRef]
66. Manoharan, P.; Boggavarapu, L.N.P.K. Improved whale optimization based band selection for hyperspectral remote sensing image classification. *Infrared Phys. Techn.* **2021**, *119*, 103948. [CrossRef]
67. Cemre, O.A.; Robiulhossain, M.Q.D.; Ali, C.G. Learning-based optimization of hyperspectral band selection for classification. *Remote Sens.* **2023**, *15*, 4460. [CrossRef]
68. Vaddi, R.; Manoharan, P. Hyperspectral remote sensing image classification using combinatorial optimisation based unsupervised band selection and CNN. *IET Image Process.* **2020**, *14*, 3909–3919. [CrossRef]

Disclaimer/Publisher's Note: The statements, opinions and data contained in all publications are solely those of the individual author(s) and contributor(s) and not of MDPI and/or the editor(s). MDPI and/or the editor(s) disclaim responsibility for any injury to people or property resulting from any ideas, methods, instructions or products referred to in the content.